Supporting Information

Light illumination and temperature induced current-voltage hysteresis in single crystal perovskite photodiodes

Juanjuan Zhou,[a] Rongzheng Ding,[a] Yingquan Peng,*[a,b] Changfeng Gu,[a] Zhuoli Zhou,[a] Wenli Lv,*[a] Sunan Xu,[a] Yi Wei[a] and Ying Wang[c]

[a] Institute of Microelectronics, College of Optical and Electronic Technology, China Jiliang University, Hangzhou 310018, China
[b] Institute of Microelectronics, School of Physical Science and Technology, Lanzhou University, Lanzhou 730000, China
[c] College of Information Engineering, China Jiliang University, Hangzhou 310018, China

*Corresponding author: E-mail: yqpeng@cjlu.edu.cn (Yingquan Peng), lvwl@cjlu.edu.cn (Wenli Lv)
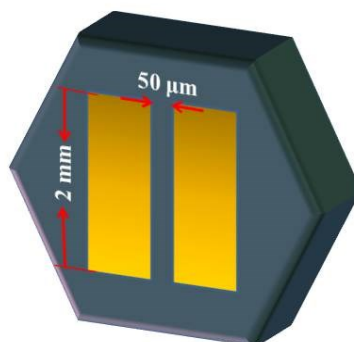
Figure S1. Device structure of the lateral diode based on single crystal $CH_3NH_3PbI_3$.

As shown in Figure S1, for photodetectors fabrication, the thicknesses of single crystals were reduced to ~ 2 mm by polish. Then Au electrodes were deposited on the (110) crystal face by vacuum thermal evaporation, in which the channel length (L) / width (W) was defined as 50 μm / 2 mm by shadow mask. Certainly, the chamber vacuum was kept at better than 5×10^{-4} Pa during Au electrodes deposition.
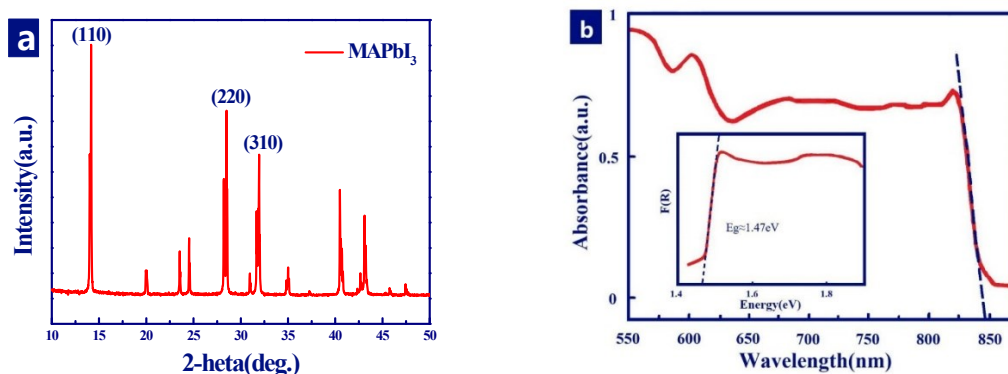

Figure S2. (a) XRD patterns spectroscopy and (b) optical absorption spectrums spectroscopy of $CH_3NH_3PbI_3$ single crystal. The inset of (b) shows the Tauc plot.

Figure S2(a) showed XRD patterns of $CH_3H_3PbI_3$ powder milled from bulk single crystal. It is clear that the sample exhibited main diffraction peaks at $2\theta = 14.14°$, $28.41°$, and $31.86°$, which corresponded to the (110), (220), and (310) reflections, respectively. Furthermore, Fig. S2(b) showed the UV-Vis-NIR absorbance spectra for $CH_3NH_3PbI_3$ perovskite. The spectra showed a clear band edge cutoff with less excitonic signature and absorption tails, which indicated the high-quality crystal of our sample with low defect concentration. The bandgap value can be obtained by Tauc equation:

$$\left(hv \cdot F(R_\infty)\right)^{1/m} = A\left(hv - E_g\right)$$

(1)

where h is the Planck's constant, $F(R_\infty)$ is Kubelka-Munk function, E_g is the bandgap value and A is the proportional constant. For $CH_3NH_3PbI_3$, a direct-bandgap semiconductor, the value of m which represents vibration frequency can be considered as 1/2. Hence, extrapolating the linear region of $\left(hv \cdot F(R_\infty)\right)^2$ to energy-axis (hv) intercept, the bandgap E_g can be obtained from Tauc plot. And the insert in Fig. S2(b) is Tauc plot, from which a bandgap E_g of 1.47 eV was obtained. Simultaneously, the synthesized single crystal also exhibits a narrower bandgap and red shifted absorption edge, which is comparable with previous reports.

The Origin of HI Definition

Generally the hysteresis is a dynamic process, and we can divide the entire hysteresis process into infinitely many static elements. That means the hysteresis can be described in the form of integral:

$$\Delta S = \int_0^{U_m} [I_r(U) - I_f(U)]dU$$

$$\bar{S} = \frac{1}{2}\int_0^{U_m} [I_r(U) + I_f(U)]dU$$

Considering the definition of hysteresis in perovskite solar cells, we revised hysteresis index (*HI*) in the diode according to the above formula:

$$HI = \frac{\Delta S}{\bar{S}} = 2\frac{\int_0^{U_m} [I_r(U) - I_f(U)]dU}{\int_0^{U_m} [I_r(U) + I_f(U)]dU}$$

$$\int_0^{U_m} I_r(U)dU \propto I_{rm} \cdot U_m$$

$$\int_0^{U_m} I_f(U)dU \propto I_{fm} \cdot U_m$$

Therefore, one obtains

2

$$\int_0^{U_m} I_r(U)dU = I_{rm} \cdot U_m \cdot \xi_r$$

$$\int_0^{U_m} I_f(U)dU = I_{fm} \cdot U_m \cdot \xi_f$$

As shown in Figure S3, we normalized the IV hysteresis curve under dark and light illumination conditions. It can be found that the curves of both Figure S3(a) and (b) under different scan rates always have overlapping parts, which means that ξ_r and ξ_f are constants that only dependent on IV curve shapes. At this point, HI can be obtained as:

$$HI = 2\frac{I_{rm} \cdot U_m \cdot \xi_r - I_{fm} \cdot U_m \cdot \xi_f}{I_{rm} \cdot U_m \cdot \xi_r + I_{fm} \cdot U_m \cdot \xi_f} = 2\frac{I_{rm} \cdot \xi_r - I_{fm} \cdot \xi_f}{I_{rm} \cdot \xi_r + I_{fm} \cdot \xi_f}$$

In the case at $\xi_r \approx \xi_f$, above equation reduces to Equation (1) to Equation (3). The same principle can also be extended to mixed hysteresis.
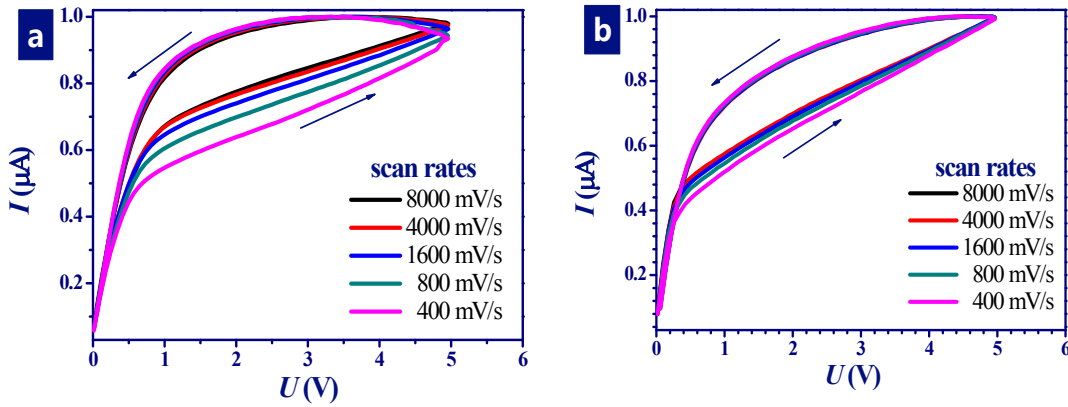

Figure S3. IV hysteresis at different scan rates (a) in the dark and (b) under light illumination of 650 nm wavelength, 0.036 mW/cm^2 intensity after normalization.